Trickle-Bed Reactor Performance

Part II. Reaction Studies

Dilute solutions (132 ppm) of formic acid in water were oxidized with air in a trickle-bed reactor at 212° to 240°C and 40 atm. Particles 0.291 and 0.0541 cm in diameter, prepared from a commercial CuO · ZnO catalyst, were used to provide a model system for studying water purification by catalytic oxidation.

Differential reactor runs were made to measure the global rate of reaction. These data were compared with predicted rates from the known intrinsic kinetics and intraparticle diffusivities, and the mass transfer coefficients measured in Part I.

High conversion (of formic acid) data were also obtained in order to test models for trickle-bed reactors. Experimental conversions agreed reasonably well (within 10%) with predicted values based upon intrinsic kinetics and the several transport rates. Axial dispersion was found to be less important than gas-to-liquid mass transfer and intraparticle diffusion. In our laboratory studies (reactor I.D. = 1 in.) careful arrangements were made to obtain nearly uniform distribution of liquid over the reactor cross section. Hence effects of maldistribution, which may be important in large-scale reactors, were minimized.

SHIEGO GOTO and J. M. SMITH

Department of Chemical Engineering
University of California
Davis, California 95616

The liquid-phase oxidation of organic pollutants in water offers the possibility of complete conversion to carbon dioxide, even for aromatic-type compounds which are resistant to biological oxidation. For example, Sadana and Katzer (1974) have reported conversions of phenol of 90% at 145°C and 17 atm oxygen pressure. Since oxygen is but slightly soluble in water, the extent of oxidation in water-full (no gas phase present) reactor operation is limited. Hence, this situation is well suited to trickle-bed operation for an adequate supply of oxygen is available in the flowing gas stream. However, predicting the performance of trickle-bed systems is complicated because interphase mass transport effects as well as kinetics of the catalytic reaction affect the conversion. The objective in Part II is to analyze experimental data obtained in a trickle-bed reactor, for the oxidation of aqueous solution of formic acid, in terms of the mass transfer and reaction processes involved. This analysis consists of two parts: First, a comparison of predicted and measured global rates of oxidation. The experimental values were obtained by operating at low conversions (differential-reactor) and the predicted values were obtained from previously determined, intrinsic kinetics (Baldi et al., 1974), for the same CuO·ZnO catalyst, and the mass transfer results of Part I. The second part is a comparison of measured high-conversion data (integral reactor) with predictions based upon models for the behavior of trickle beds.

Published studies on trickle-bed reactors are meager. Hartman and Coughlin (1972) investigated the oxidation of SO_2 at 1 atm and 22°C with activated carbon particles as the catalyst. Their results showed that both mass transfer of oxygen from the gas phase and the intrinsic reaction rate affected the performance; a single rate process could not describe the data. Particularly lacking is information on trickle-bed reactors operated under pressure. Qualitative and overall performance considerations are discussed by Hoog et al. (1953) and Ross (1965), but procedures for reactor design are not considered.

Two related studies are significant. Satterfield and Way (1972) studied the effect of an inert liquid, flowing over the silica-alumina catalyst particles, on the gas-phase isomerization of cyclopropane at 1 atm and 50° to 120°C. Their results showed that intraparticle and external diffusion resistances were more important in a trickle-bed reactor than for the gas-solid catalytic system. Similarly, Sedricks and Kenney (1973) found that liquid wetting of the catalyst particles reduced the global rate of reduction of crotonaldehyde (at 31°C and 1 atm) with palladium/Al_2O_3. Presumably this reduction was due to increased mass transfer resistances when liquid wet the particles. The results reported here agree with these separate observations in that gas-to-liquid, and liquid-to-solid mass transfer, intraparticle diffusion, and intrinsic kinetics are all shown to affect the global rate of oxidation of formic acid.

EXPERIMENT

Apparatus

Both rates and integral reactor conversions were measured in the same apparatus, shown in Figure 1, by varying the

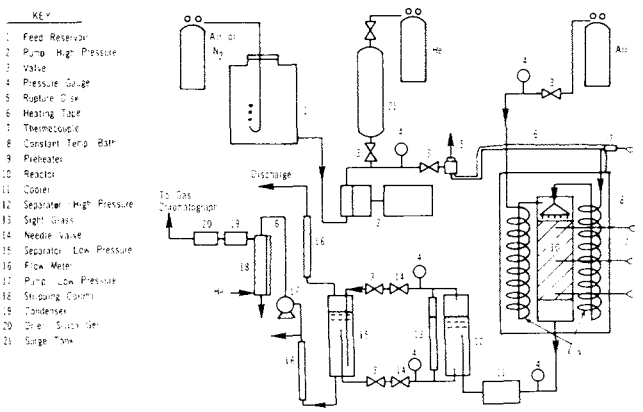

Fig. 1. Apparatus for reaction data.

Correspondence concerning this paper should be addressed to J. M. Smith. S. Goto is on leave from University of Nagoya, Japan.

amount of catalyst. Water containing 28.7×10^{-7} g moles/cm³ (132 ppm) of formic acid was saturated with air at atmospheric pressure and 25°C, $C_{L,O_2} = 2.70 \times 10^{-7}$ g mole/cm³, in reservoir (1) and then fed to the reactor (10) at 40-atm pressure with a diaphragm-type stainless steel metering pump (2). This pump [Whitey model LP (10)] gave very small pressure fluctuations in the discharge stream. The feed solution was heated to operating temperature (212° to 240°C) with an electric preheater (6) and a coil immersed in the constant-temperature air bath (8) containing the reactor. The gas stream was air, preheated by flowing through a similar coil.

The reactor was made of a 12-in. section of 1-in. I.D. stainless steel tubing. The liquid was introduced through the distributor described in Part I. The catalyst was supported by a stainless steel screen placed near the bottom of the reactor. The bottom of the capillary tubes in the distributor were located 0.2 cm above the top of the catalyst bed to avoid end effects as far as possible. Temperatures were measured with iron-constantan thermocouples at three axial locations (3 in., 5.5 in., and 8 in.) down from the top of the reactor and in the water feed. Since formic acid concentrations were low, the temperature rise due to reaction was negligible. The thermocouple in the water feed read within 2°C of the three couples in the reactor.

The effluent was cooled to room temperature (11) and separated into gas and liquid phases in a high-pressure separator (12) made of 1.5-in. I.D. stainless steel tubing. Needle valves (14) were used to control the gas and liquid flow rates to maintain a constant level in the separator (12). Dissolved gases were evolved when the liquid flowed through the needle valve. This gas was separated from the liquid in a 1.6-in. I.D. glass tube (15) operated at about atmospheric pressure. The gas stream from the high-pressure separator was added through a dispersion tube into the liquid in the low-pressure separator so that equilibrium could be approached for the gas and liquid phases leaving the low-pressure separator. Then it was not necessary to analyze the gas phase. This two-separator procedure was a satisfactory, low-cost solution for the rather difficult experimental problem of controlling pressure and flow rates in a high-pressure, trickle-bed reactor.

Flow rates of the gas and liquid streams from the low-pressure separator were measured and the gas stream discharged. Part of the liquid stream flowed to a stripping column (18) where CO_2 and O_2 were removed with helium and passed to a gas chromatograph for analysis.

Analysis Procedure

Since the oxidation of formic acid involves no stable intermediates, the rate of production of carbon dioxide is a measure of the rate of disappearance of formic acid (or oxygen). Carbon dioxide is present in both the liquid and gas streams from the low-pressure separator. However, if equilibrium exists in this separator, the total production of CO_2 can be determined from the flow rates of both phases and the CO_2 content of the liquid.

To test the approach to equilibrium, the equipment was operated with a liquid feed of distilled water saturated with CO_2 and a gas stream of CO_2-free air. If equilibrium is achieved, a mass balance for CO_2 gives

$$(C_{L,CO_2})_e = \frac{F_L (C_{L,CO_2})_f}{F_L + H_{CO_2} F_g} \qquad (1)$$

where $(C_{L,CO_2})_f$ is the concentration in the feed, $(C_{L,CO_2})_e$ the concentration in the liquid from the separator, and H_{CO_2} is Henry's law constant. The latter quantity for CO_2 is 1.20 [mole/(cm³ of gas)]/[mole/(cm³ of liquid)] at 25°C (Perry, 1963). Values of $(C_{L,CO_2})_e$ calculated from Equation (1) are compared with the concentrations determined from the chromatographic analysis in Table 1. The results indicate that equilibrium in the low-pressure separator is a valid assumption.

Rates of reaction and conversions of formic acid were determined from the total CO_2 production in the gas and liquid streams. As an overall check, a mass balance of carbon was made for a few runs. A Beckman TOC (total organic carbon) analyzer was used to determine the total carbon in the liquid feed (due to formic acid and dissolved CO_2). The gas stream was free of carbon. The total carbon in the liquid from the low-pressure separator was measured in the TOC instrument. The CO_2 in the gas stream was evaluated, by assuming equilibrium, from the chromatographic analysis of the liquid. The total carbon in the feed and in the effluent streams agreed within 5%.

Table 1. Approach to Equilibrium in Low-Pressure Separator

F_L cm³/s	F_g cm³/s	$(C_{L,CO_2})_f \times 10^5$ g mole/cm³	$(C_{L,CO_2})_e \times 10^5$ g mole/cm³ Exp.	Calc., Equation (1)
0.9	4.0	3.32	0.503	0.524
1.8	4.0	3.32	0.956	0.905

Table 2. Range of Operating Conditions

1. Mass of catalyst in bed, g	
for differential reactor	2.0 ($d_p = 0.0541$) and 5.05 ($d_p = 0.291$)
for integral reactor	19.5 ($d_p = 0.0541$) and 49.8 ($d_p = 0.291$)
2. Catalyst particle size, d_p	
average diameter, cm	0.0541[a], 0.291[b]
3. Liquid flow rate, cm³/s	0.45, 0.90, 1.35, 1.80
4. Gas flow rate, cm³/s[c]	0, 1.0, 2.0, 4.0
5. Temperature, °C	212°, 224°, 232°, 240°
6. Feed concentrations in water	
Oxygen, g mole/cm³	2.70×10^{-7}
Formic acid, g mole/cm³	28.7×10^{-7}
7. Pressure, atm	40

[a] 28 to 32 mesh.
[b] Pie-shaped quarters of ¼ in. × ⅛ in. cylindrical pellets.
[c] At 25°C and 1 atm.

The variables studied in both differential and integral reactor runs were liquid and gas flow rates, temperature, and catalyst particle size, as shown in Table 2. The effects of formic acid and oxygen concentrations, and temperature, on the intrinsic rate have been determined (Baldi et al., 1974) for the same catalyst, a commercial (G-66B, Chemetron Corporation) material containing 82.5 wt % ZnO and 16.5 wt % CuO and with a surface area and porosity of 35.9 m²/g and 0.56.

Catalyst Pretreatment

To obtain reproducible data it was necessary to pretreat the catalyst by passing a nearly oxygen-free solution of formic acid through the reactor for 10 hours at 240°C and 40 atm pressure. During this pretreatment, which is described in detail by Baldi et al. (1974), the reactor was operated liquid full. Then the feed was changed to air and air-saturated formic acid solution. After 4 hours, reproducible results could be obtained for on-stream times up to at least 60 hours.

MASS TRANSFER RATE PARAMETERS AND PROPERTIES

In order to predict global rates of reaction and conversion in trickle-bed reactors it is necessary to know $k_L a$, $k_s a$, E_f (see Part I for Notation) as well as the intrinsic rate, all at reactor operating conditions. The mass transfer coefficients were measured in Part I, but at 25°C and 1 atm. To obtain these coefficients at 40 atm and temperatures from 212° to 240°C, the correlations of the low-pressure data of Part I, Equations (17) and (22), with the experimental values of α_L, n_L, α_s, and n_s were used. This required densities and viscosities for water, and diffusivities of oxygen and formic acid in water, at 40 atm. These properties were estimated from data and correlations in the

Table 3. Density, Viscosity and Diffusivities in Water at 40 Atm Pressure

t, °C	ρ, g/cm³	μ, g/(cm)s	D_{O_2}, cm²/s	D_{FA}, cm²/s	H_{O_2}[a]
212	0.850	1.10×10^{-3}	2.86×10^{-4}	2.29×10^{-4}	1.56
224	0.837	1.03×10^{-3}	2.98×10^{-4}	2.39×10^{-4}	1.92
232	0.827	0.98×10^{-3}	3.22×10^{-4}	2.58×10^{-4}	2.45
240	0.794	0.92×10^{-3}	3.40×10^{-4}	2.73×10^{-4}	3.82

[a] [g mole/(cm³ of gas at 25°C, 1 atm)]/[g mole/(cm³ of liquid at 40 atm and t)].

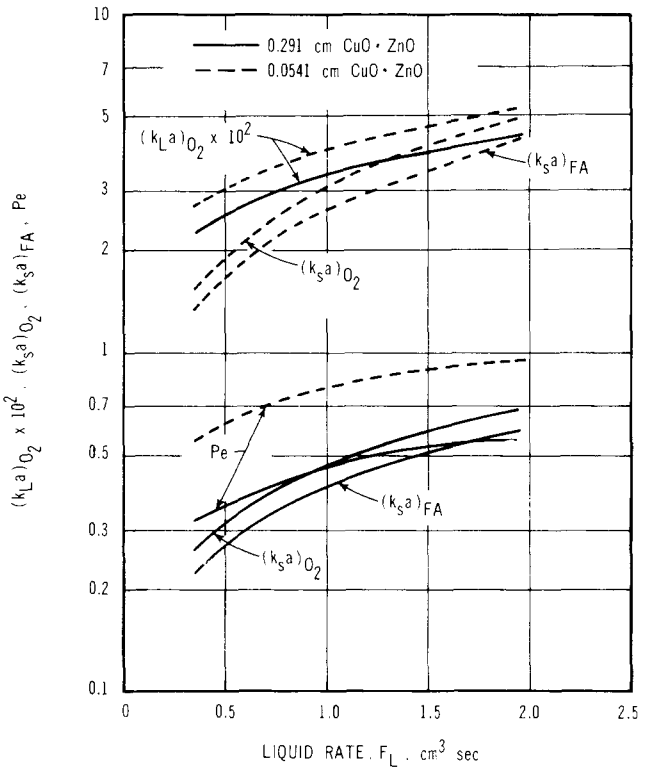

Fig. 2. Predicted rate coefficients at 240°C, 40 atm.

literature (Perry, 1963; Washburn, 1929; Hougen and Watson, 1947; Othmer and Thaker equation, Reid and Sherwood, 1966). The Henry-law constant for oxygen is also needed. It was obtained from the data of Himmelblau (1960). These properties at 40 atm are listed in Table 3. The resultant values of k_La and k_sa for oxygen and formic acid are illustrated in Figure 2 for 240°C. Similar results were obtained at other temperatures.

If axial dispersion is accounted for in the liquid phase in the reactor model, the dispersion coefficient, E, for oxygen and formic acid in water is needed. The correlation of Furzer and Michell (1970) was used to estimate E. In terms of superficial values of the velocity and E, their correlation may be written

$$Pe = \frac{d_p u_L}{E} = 4.3 \left(\frac{Re}{H_d}\right)^{1/2} (Ga)^{-1/3} \qquad (2)$$

The dynamic holdup was estimated from the experimental data of Part I using Equation (5) with the appropriate values of A for the CuO·ZnO particles. The Peclet numbers applicable at 40 atm and 240°C are also shown in Figure 2.

To account for intraparticle diffusion the effective diffusivities, D_{e,O_2}, $D_{e,FA}$ and intrinsic rate constant $k_{O_2}^*$ are needed. These quantities for oxygen were measured at various temperatures by Baldi et al. (1974) (Table 1) for the same catalyst in a liquid-full reactor. The effective diffusivity for formic acid was calculated from D_{e,O_2} by supposing that the tortuosity factor is independent of the diffusing component; that is, $D_{e,FA} = D_{e,O_2}\,(D_{FA}/D_{O_2})$.

DIFFERENTIAL REACTOR RESULTS

For the global rate measurements small amounts of catalyst were employed (Table 2) giving conversions from 4 to 22% for formic acid and 0.15 to 2.3% for oxygen. Experimental values for the rates were obtained from the measured feed and exit concentrations of CO_2 using the equation

$$-2R_{O_2} = R_{CO_2} = [(F_L + H_{CO_2}F_g)(C_{L,CO_2})_e - F_L(C_{L,CO_2})_f]/W \qquad (3)$$

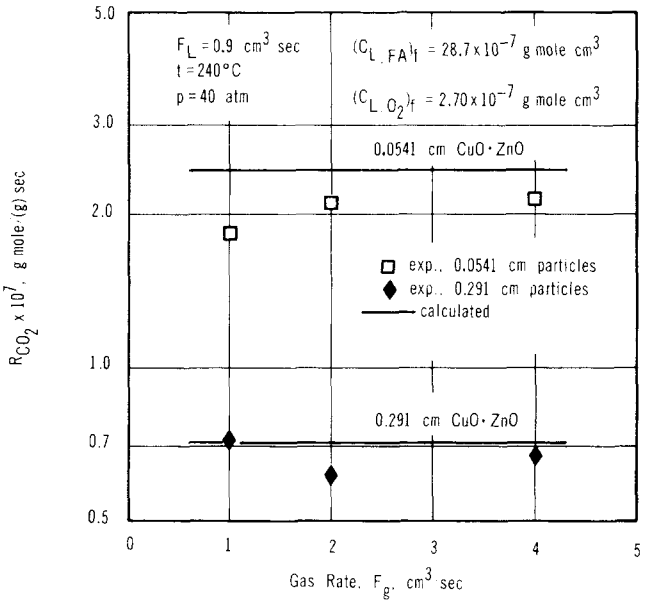

Fig. 3. Effect of gas rate on global rate in a differential trickle-bed reactor.

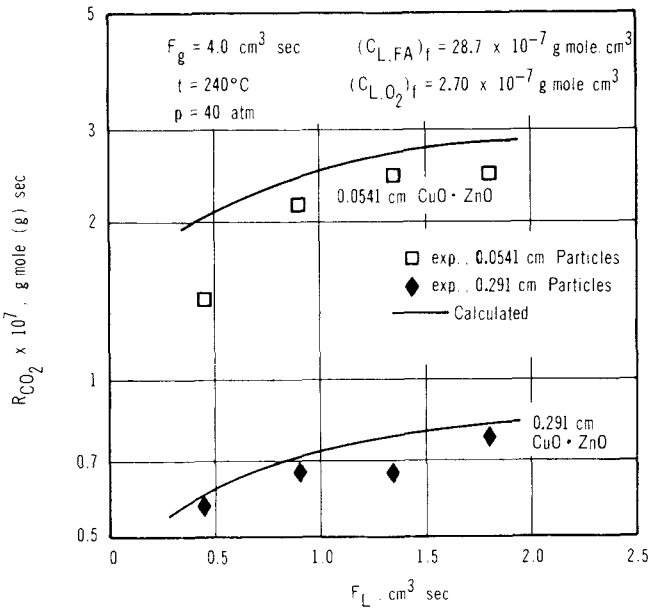

Fig. 4. Effect of liquid rate on global rate in differential trickle-bed reactor.

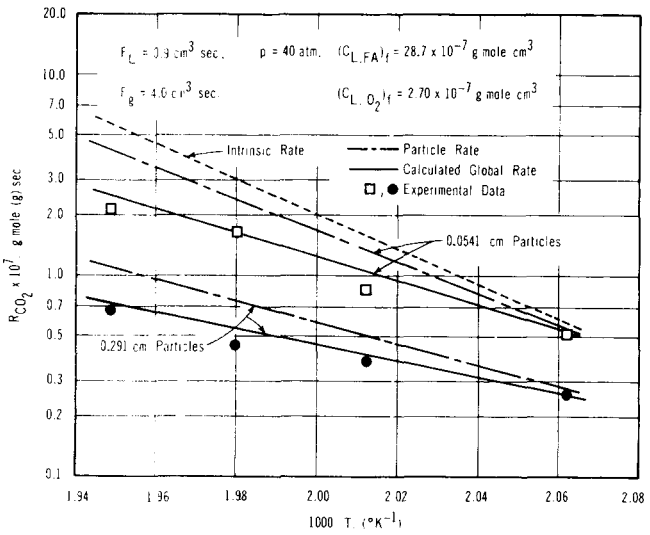

Fig. 5. Effect of temperature on the global rate in a differential trickle-bed reactor.

Using CO_2 concentrations was more accurate than calculations based upon oxygen concentrations because $(C_{L,CO_2})_f$ was nearly zero, while the oxygen concentrations in feed and exit streams were of the same magnitude. The data points in Figures 3 to 5 show the effects of F_g, F_L and temperature on the global rates. The rate was independent of gas flow rate but increased with F_L in agreement with the results in Part I where k_La and k_sa were found to be independent of F_g but an increasing function of the liquid rate (Figures 6 and 8 of Part I). The large difference in rates for the two sizes of particles is due primarily to intraparticle diffusion resistances.

Calculated values for the global rate were obtained from the feed concentrations of oxygen and formic acid, and k_La, k_sa, and E_f by writing mass balances for oxygen and formic acid in the liquid phase. The problem is to evaluate surface concentrations C_{s,O_2} and $C_{s,FA}$ so that the intrinsic rate equation can be used. Baldi et al. (1974) found that the intrinsic rate was first order in oxygen and formic acid so that for the catalyst particle

$$-R_{O_2} = k_{O_2}^{*}\, E_f\, (C_{s,FA})\,(C_{s,O_2}) \tag{4}$$

The mass balances in the liquid may be written in terms of feed concentrations as follows:

$$F_L[(C_{L,O_2})_f - C_{L,O_2}] + k_La\, Sz_B\, (C^{*}_{L,O_2} - C_{L,O_2}) - (k_sa)_{O_2}\, Sz_B\, (C_{L,O_2} - C_{s,O_2}) = 0 \tag{5}$$

and

$$F_L[(C_{L,FA})_f - C_{L,FA}] - (k_sa)_{FA}\, Sz_B\, (C_{L,FA} - C_{s,FA}) = 0 \tag{6}$$

where C_{L,O_2} and $C_{L,FA}$ and C_{s,O_2} and $C_{s,FA}$ are bulk and surface concentrations in the reactor. Since the conversion is small, these concentrations are assumed to be constant in the reactor. Such bulk concentrations are related to the surface concentrations by the following boundary conditions:

$$(k_sa)_{O_2}\,(C_{L,O_2} - C_{s,O_2}) = k_{O_2}^{*}\, E_f\, \rho_B\, C_{s,O_2}\, C_{s,FA} \tag{7}$$

$$(k_sa)_{FA}\,(C_{F,LA} - C_{s,FA}) = 2k_{O_2}^{*}\, E_f\, \rho_B\, C_{s,O_2}\, C_{s,FA} \tag{8}$$

The effectiveness factor E_f cannot be expressed rigorously as an explicit function of C_{s,O_2} because Equation (4) is nonlinear. However, Bischoff (1965) has shown that E_f is given to a good approximation by the equations

$$E_f = \frac{1}{m}\left[\frac{1}{\tanh 3m} - \frac{1}{3m}\right] \tag{9}$$

$$\hat{m} = \frac{V_p}{S_p} R_s \left[2\int_0^{C_s} D_e\, R\, dC\right]^{-1/2} \tag{10}$$

where R is the intrinsic rate of reaction and C is the concentration of the limiting component. Using Equation (4) with $E_f = 1.0$ for the intrinsic rate, Equation (10) becomes

$$\hat{m} = \frac{d_p}{6}\left[\frac{k_{O_2}^{*}\, \rho_p\, C_{s,FA}}{D_{e,O_2}\,(1 - B/3)}\right]^{1/2} \tag{11}$$

for oxygen as the limiting component ($B \leq 1$), and

$$\hat{m} = \frac{d_p}{6}\left[\frac{2k_{O_2}^{*}\, \rho_p\, C_{s,O_2}}{D_{e,FA}\,(1 - 1/3B)}\right]^{1/2} \tag{12}$$

for formic acid as the limiting component ($B > 1$), where B is the ratio $2D_{O_2}\, C_{s,O_2}/D_{FA}\, C_{s,FA}$. For known values of $(C_{L,O_2})_f$ and $(C_{L,FA})_f$, $k_{O_2}^{*}$, D_{e,O_2}, and $D_{e,FA}$, Equations (5) to (9) and (11) or (12) can be solved by trial for the six unknowns C_{L,O_2}, $C_{L,FA}$, C_{s,O_2}, $C_{s,FA}$, $\hat{m}$, and E_f. Knowing the values of C_{s,O_2} and $C_{s,FA}$, we can calculate the global rate R from Equation (4). The solid curves in Figures 3 to 5 show such calculated rates for comparison with the experimental global rates. This comparison is a measure of the overall consistency of the intrinsic rate data and D_e values, the mass transfer results in Part I, and the accuracy of the estimates of properties at 40 atm and elevated temperatures (Table 3). Since these are completely independent sets of data, the agreement is reasonably good. The derivations between experimental and predicted rates is probably due primarily to uncertainties in estimating diffusivities at 40 atm and 212° to 240°C.

In order to compare the effects of intraparticle and external diffusion on the global rate, the upper, dotted line in Figure 5 has been included to show the intrinsic reaction rate evaluated at bulk concentrations, C_{L,O_2} and $C_{L,FA}$. This rate is independent of catalyst particle size. The dashed lines represent the particle rate, that is, the rate when surface concentrations are equal to the bulk values; that is, these lines are for rates that include intraparticle diffusion retardation but not the external diffusional effects associated with k_La and k_sa. The difference between dotted and dashed lines for a given particle size show the retardation of the rate due to intraparticle diffusion, while the difference between dashed and solid lines represents the importance of k_La and k_sa. It is clear that even for the small, 0.0541-cm particles that all mass transfer resistances are significant.

INTEGRAL REACTOR (HIGH CONVERSION) RESULTS

In order to evaluate reactor models for trickle-bed operation with uniform liquid distribution, experimental data were obtained for catalyst beds containing large amounts of catalyst (Table 2) so that high conversions (60% to 97%) of formic acid were obtained. Measurements were made at 240°C for both catalyst sizes over a range of gas and liquid flow rates. Experimental values of the formic acid conversion were evaluated from the flow rates of both streams and composition data using the equation

$$x_{FA} = \frac{(F_L + H_{CO_2} F_g)\,(C_{L,CO_2})_e - F_L(C_{L,CO_2})_f}{F_L(C_{L,FA})_f} \tag{13}$$

The data points in Figures 6 and 7 show these experimental results.

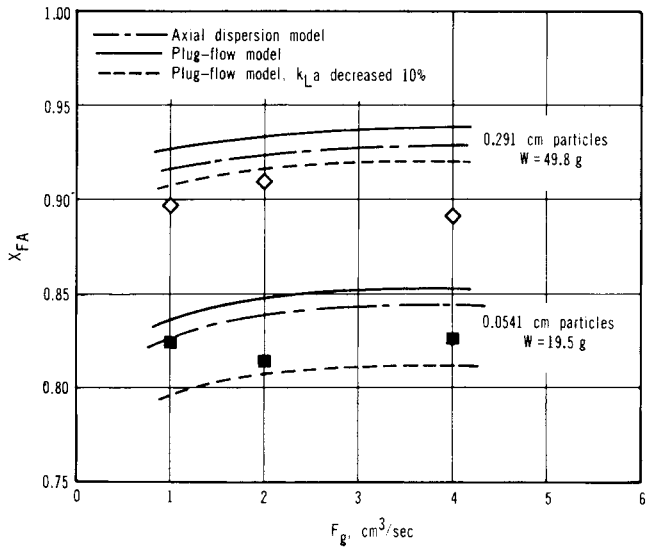

Fig. 6. Effect of gas flow rate on conversion of formic acid; integral trickle-bed reactor (F_L = 0.9 cm³/s, t = 240°C, p = 40 atm).

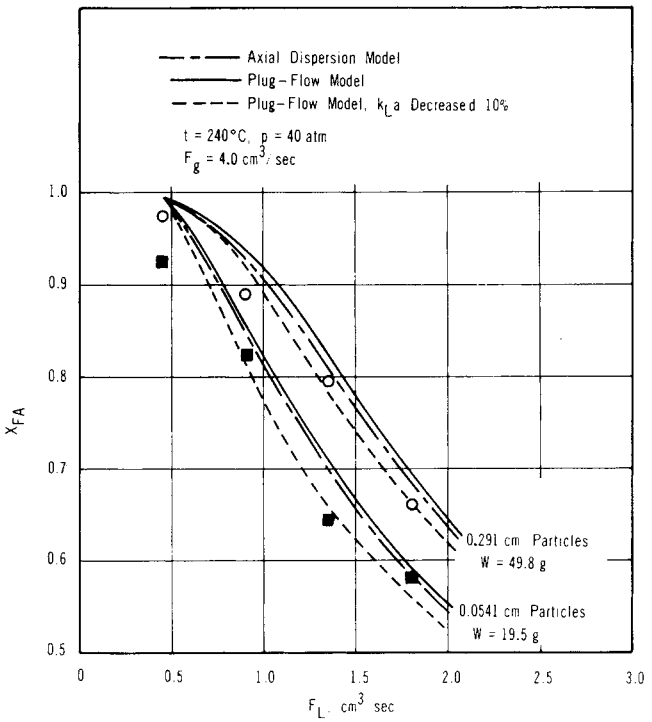

Fig. 7. Effect of liquid flow rate on conversion of formic acid; integral trickle-bed reactor.

Conversions were predicted using axial dispersion and plug-flow models for the liquid phase. The primary assumptions in both of these models are that:

1. Axial dispersion in the gas phase is negligible,
2. Conditions are uniform in the radial direction,
3. Gas and liquid flow rates are constant throughout the reactor,
4. Mass transfer resistance in the gas phase is negligible, as ascertained for oxygen in Part I, so that equilibrium exists at the gas-liquid interface,
5. Intrinsic reaction rate and intraparticle diffusivity are the same as determined previously, Baldi et al. (1974), for liquid-full reactor conditions.

Axial Dispersion Model

If axial dispersion in the liquid phase is described by the dispersion coefficient E, differential mass balances for oxygen and formic acid in the liquid and gas phases are:
Oxygen in the gas phase:

$$F_g \frac{d\,C_{g,O_2}}{dz} + (k_La)_{O_2} S(C^*_{L,O_2} - C_{L,O_2}) = 0 \quad (14)$$

Oxygen in the liquid phase:

$$ES \frac{d^2C_{L,O_2}}{dz^2} - F_L \frac{d\,C_{L,O_2}}{dz} + (k_La)_{O_2} S(C^*_{L,O_2} - C_{L,O_2}) - (k_sa)_{O_2} S(C_{L,O_2} - C_{s,O_2}) = 0 \quad (15)$$

Formic acid:

$$ES \frac{d^2C_{L,FA}}{dz^2} - F_L \frac{dC_{L,FA}}{dz} - (k_sa)_{FA} S(C_{L,FA} - C_{s,FA}) = 0 \quad (16)$$

The axial dispersion coefficient is a function of the holdup and was obtained from Equation (2).

Equations (7) and (8) are applicable as well as the following boundary conditions:

at $z = 0$

$$C_{g,O_2} = (C_{g,O_2})_f \quad (17)$$

$$-ES \frac{dC_{L,O_2}}{dz} = F_L[(C_{L,O_2})_f - C_{L,O_2}] \quad (18)$$

$$-ES \frac{dC_{L,FA}}{dz} = F_L[(C_{L,FA})_f - C_{L,FA}] \quad (19)$$

at $z = z_B$

$$\frac{dC_{L,O_2}}{dz} = 0 \quad (20)$$

$$\frac{dC_{L,FA}}{dz} = 0 \quad (21)$$

The equilibrium concentration of oxygen in the liquid is related to the gas concentration by Henry's law:

$$C^*_{L,O_2} = C_{g,O_2}/H_{O_2} \quad (22)$$

Equations (9) and (11) or (12) relate the effectiveness factor and concentrations at the outer surface of the catalyst particles.

Equations (14) to (22) with (7), (8), (9), and (11) or (12) can be solved numerically to obtain axial profiles for the concentrations and the conversion of formic acid. A procedure which does not require excessive computer time is as follows:

1. At $z = z_B$ assume values for C_{g,O_2}, C_{L,O_2}, and $C_{L,FA}$.
2. Starting at z_B integrate Equations (14) to (16) numerically using boundary conditions given by Equations (20) and (21). For the step-wise integration to $z = 0$, the Runge-Kutta-Gill method (Ralston and Wilf, 1960) was used.
3. The assumed concentrations at z_B were checked by noting if the calculated concentrations at $z = 0$ satisfied Equations (17) to (19).

Plug-Flow Model

If axial dispersion in the liquid is neglected, the calculations are markedly simplified because the two-point boundary value problem is eliminated. For this model the second derivative terms in Equations (15) and (16) are eliminated and the boundary conditions, Equations (18) to (21), are replaced by the following known conditions at $z = 0$.

$$C_{L,O_2} = (C_{L,O_2})_f \quad (22)$$

$$C_{L,FA} = (C_{L,FA})_f \quad (23)$$

In the plug-flow model, the liquid holdup is not involved.

Comparison of Experimental and Predicted Results

The solid and dotted lines in Figures 6 and 7 show that the conversions predicted by the axial dispersion and plug-flow models differ by only about 2%. Predicted results are higher by 0 to 5% than the experimental conversions although the deviations are less for the axial dispersion model. In the model calculations, the estimated values for k_La and k_sa and the intrinsic rate equation were used, rather than the experimentally determined global rates. This was done in order to test the complete calculations starting with the intrinsic rate and mass transfer correlations. As Figures 3 and 4 show, predicted global rates were higher than the experimental values. Hence, the deviations between predicted and experimental values in Figures 6 and 7 would appear to be due to errors in the global rate rather than to inadequacies in the models. As mentioned, the differences between the experimental and predicted rates shown in Figures 3 and 4 are probably caused by uncertainties in the values of the diffusivities and viscosities at 40 atm and 212° to 240°C.

Figures 8 and 9 show the calculated, dimensionless concentration profiles through the reactor for oxygen (gas and liquid phases) and formic acid, and the effectiveness factors. Analysis of these curves indicates that all the transport processes retard the conversion, except the transfer of oxygen from gas to gas-liquid interface. The values for Y_{L,O_2} $[= C_{L,O_2}/(C^*_{L,O_2})_f]$ are much less than unity at the reactor entrance, which illustrates the large effect k_La has on the conversion. The differences between the curves for surface and bulk-liquid concentrations show that the effect of k_sa, while significant, is less than that of k_La. The effectiveness factors for the 0.291-cm particles are from 0.2 to 0.3, and even for the 0.0541-cm particles E_f is from 0.7 to 0.9. The large effects of k_La and E_f arise because of the low solubility of oxygen in water and the low molecular diffusivities in liquids. These factors predominate even though the intrinsic rate is not particularly rapid.

The flat curves for Y_{g,O_2} in Figures 8 and 9, which are essentially the same for both models, show that the oxygen is not significantly depleted; that is, an excess of oxygen always was present in the gas phase. The decrease in the curves for Y_{L,O_2} in the first part of the reactor in Figure 9 shows that oxygen is reacting faster than it is transferred from the gas phase to the liquid. Since the intrinsic reaction is second order, this situation is reversed at higher conversions and the oxygen concentration builds up in the last part of the reactor. In Figure 8 for the larger particles, the rate of reaction is lower so that the initial decrease in Y_{L,O_2} does not occur.

DISCUSSION

The relative importance of the four transport resistances in our laboratory, trickle-bed reactor with uniform distribution of liquid is, in decreasing order: gas-to-liquid, k_La; intraparticle diffusion, E_f; liquid-to-particle, k_sa; and axial dispersion. This order is interesting in that the largest significance for k_La is in contrast to the often-mentioned criterion that intraparticle diffusion is more important than external mass transfer. However, the criterion was developed for single-fluid flow, as in gas-solid catalytic reactors, rather than for two fluid phases. To illustrate the large effect of gas-to-liquid transport, the dotted lines in Figure 10 show the concentration profiles corresponding to $k_La = \infty$, while the solid lines are based on the predicted values of k_La, both for the plug flow model. For $k_La = \infty$, the oxygen in the liquid is in equilibrium with that in the gas. This results in a high liquid concentration and reaction rate. Then the formic acid concentration falls sharply in the first part of the reactor. Complete conversion would be achieved after 6 cm of catalyst bed. Both oxygen and formic acid profiles are decidedly different than for the real case (*solid lines in Figure 10*).

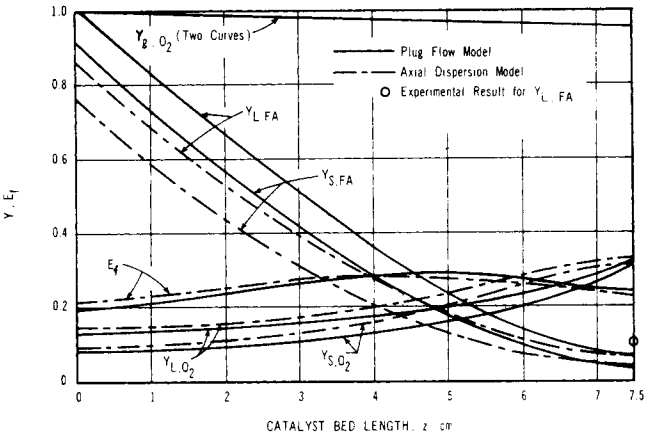

Fig. 8. Axial concentration profiles (d_p = 0.291 cm, F_L = 0.9 cm³/s, F_g = 4.0 cm³/s, t = 240°C, p = 40 atm).

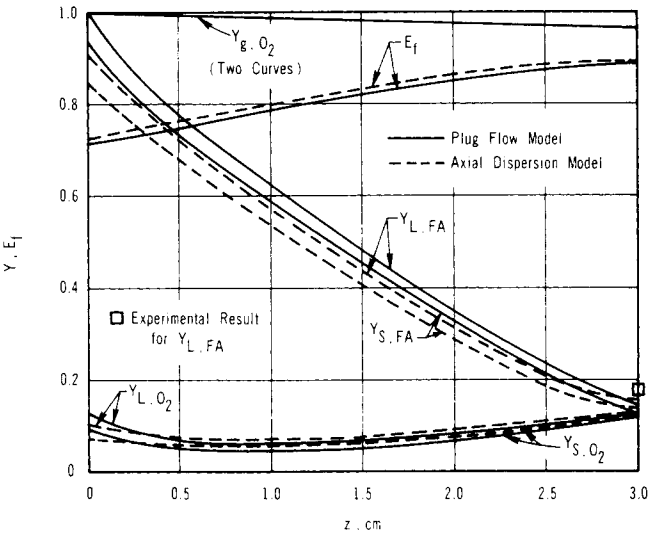

Fig. 9. Axial concentration profiles (d_p = 0.0541 cm, F_L = 0.9 cm³/s, F_g = 4.0 cm³/s, T = 240°C, p = 40 atm).

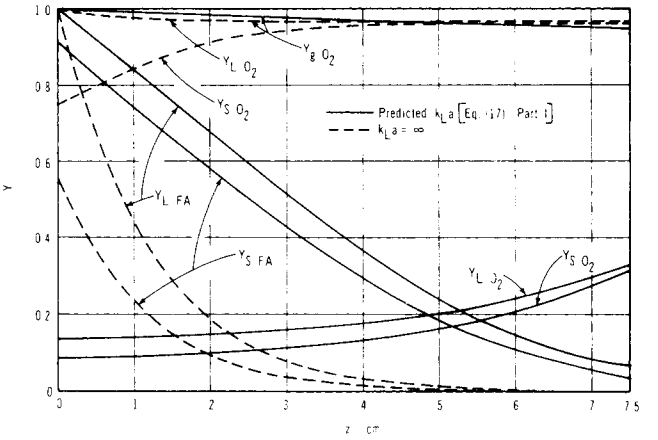

Fig. 10. Effect of gas-to-liquid mass transport, plug-flow model (d_p = 0.291 cm, F_L = 0.9 cm³/s, F_g = 4.0 cm³/s t = 240°C, p = 40 atm).

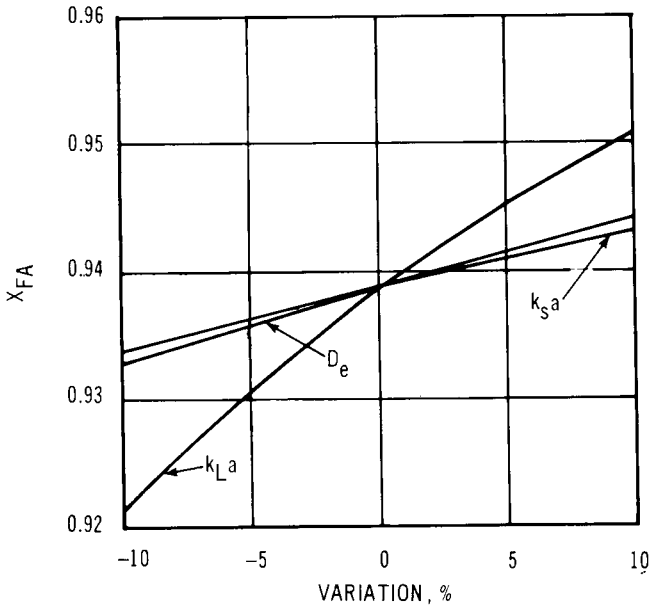

Fig. 11. Sensitivity of conversion to rate coefficients (F_L = 0.9 and F_g = 4.0 cm³/s, d_p = 0.291 cm, t = 240°C, p = 40 atm).

The quantitative effect on the conversion of the three local transport processes is shown in Figure 11. Here the usual values of k_La, k_sa and D_e are used in the computations, except one of them is varied by the amount indicated on the abscissa. The ordinate values show the corresponding change in conversion. The dominating effect of k_La is again evident. Since k_La is dependent upon the somewhat uncertain estimates of diffusivities, it is not unlikely that the predicted values for this rate coefficient are in error. The calculations for the conversion shown in Figure 11 for a 10% lower value of k_La, for one particle size and set of flow rates, were repeated for other conditions using the plug-flow model. The results are indicated by the dotted lines in Figures 6 and 7. Comparison with the solid lines shows that a 10% error in k_La has a greater effect than inclusion of axial dispersion in the model. Also a 10% error in k_La is enough to account for the difference between predicted and experimental conversions. It should be noted that the restriction in our work to uniform liquid distribution poses important limitations in using the results for scale-up. Nonuniform distribution is normal in large-diameter reactors, and this can affect performance significantly, particularly at high conversions. Also scale-up may lead to linear liquid velocities much different than those employed in our work. At widely different velocities the flow regime in the reactor may be different (Weekman and Myers, 1964) with probably different mass transfer coefficients. For example, axial dispersion and reduction in effective mass transfer area (due to inadequate wetting of the particles) could be much more important at very low liquid velocities.

ACKNOWLEDGMENT

The financial assistance of the Water Resources Center, University of California, Grant W-392, is gratefully acknowledged. The ZnO·CuO catalyst was supplied by the Chemetron Corporation.

NOTATION

(See Part I).

LITERATURE CITED

(See Part I).

Manuscript received December 2, 1974; revision received February 3 and accepted February 14, 1975.

Stresses and Friction Forces in Moving Packed Beds

A model to determine stresses and friction forces in moving packed beds with interstitial fluid flow has been developed. The scaling parameters are determined from the governing equations. A plane and an axisymmetric bed geometry are studied and the wall stress calculated under uniform one-dimensional axial flow conditions. The effect of added transverse flow (for example, due to a screen in the wall) is investigated. The present model is an improvement over earlier, one-dimensional models with capability to include in the stress analysis varying pressure gradients in all directions which may exist in practical moving bed systems.

GERSHON GROSSMAN

Faculty of Mechanical Engineering
Technion—Israel Institute of Technology
Haifa, Israel

SCOPE

Packed beds of granular solids flowing through a column as a consolidated plug have had wide application in chemical and physical processes involving solid-fluid interactions. While most such systems have relied on gravity-induced motion of the bed (with co-flow or counterflow of the contacting fluid), there has been growing interest in recent years in utilizing the fluid drag of the co-flow as a driving force for the bed, which provides for better control and higher bed velocities. The moving bed idea has been applied to the design of several continuous and semi-continuous solid-liquid contactors for processes such as crystal washing and ion exchange (Aerhart et al., 1956; Hancher and Jury, 1959; Shwartz and Probstein, 1969; Gold et al., 1971, 1973).

In many of the moving bed systems, especially in those with fluid counterflow, difficulties have been encountered